

The Statistical Analysis of Noise in Triaxial Magnetometers and Calibration Procedure

Nhan Nguyen, Philipp Müller, and Jussi Collin

Faculty of Information Technology and Communication Sciences (ITC)

Tampere University

FI-33014 Tampere University, Finland

nhan.nguyen@tuni.fi, philipp.muller@tuni.fi, jussi.collin@tuni.fi

Abstract—This paper examines the statistical behaviour of noise in triaxial sensors, particularly magnetometers. It is shown by statistical test that the sensor noise does not follow a Normal distribution as is commonly assumed. Beside noise, other sources of error in readings of magnetometers are discussed. The combined effects of errors are demonstrated by a mathematical model, which helps calibrating magnetometer readings under the Maximum Likelihood Estimator scheme. Calibrated data is aligned to the sensor frame in order to be applied later in navigation applications, where the North finding problem is solved by true geomagnetic readings.

Index Terms—Statistical Analysis, Inertial Navigation, Sensor Noise, Magnetometers, Calibration

I. INTRODUCTION

Smartphone usage for pedestrian navigation has increased dramatically in recent years. In order to provide the user with an exact route to a new place, one of the challenges is to get an estimate for the smartphone's orientation. The orientation of the phone with respect to vectors of the Earth's gravity and magnetic field can be estimated using observations from accelerometer and magnetometer. However, low-cost magnetometers in smartphones are affected by several sources of errors and by induced noise, e.g. due to manufacturing limitation and magnetic distortion in the vicinity of the sensors. Thus, magnetic field sensors need calibrating before they can be used for any applications.

Multiple approaches have been introduced to calibrate the magnetometers. The initial proposal was to put the magnetic sensor through a swinging process [1]. This technique requires to put the sensor set in several known orientations, take measurements, and compare them with reference measurements. The problem of aligning the set to known orientations accurately has been discussed in [2] and [3].

The second method set, namely "attitude-dependent", is created to calibrate the magnetometers by using external heading information [4]. However, the need for external information regularly is the main limitation of these methods.

This research was financially supported by Business Finland (Autoport project, decision number 7567/31/2018) and the Faculty of Information Technology and Communication Sciences at Tampere University, Finland.

The "attitude-independent" methods, which calibrate magnetometers without heading information, try to fit the measurements to an elliptical manifold. The batch least squares calibration algorithm derived in [2] solves the non-orthogonality, scaling and bias errors of magnetometers. In [3], the inconsistency of this algorithm in estimating error parameters of the sensors is discussed, and the Adaptive Least Squares algorithm for tackling the problem is proposed.

Among recent articles, [5] is one of the first papers tackling the statistical property of noise in sensor. The derived calibration algorithm which is based on the Maximum Likelihood Estimator [MLE] framework to estimate the error parameters is shown to be robust from the statistical point of view. The algorithm in [5] constantly requires the external information sources to align calibration readings to the sensor frame. Inspired by the method, this paper reviews the magnetometer error model and algorithm to calibrate the readings based on this model within MLE framework. Furthermore, this paper shows, using simulated data, that the external information sources are only needed for a short time interval while the algorithm can still self align.

To the authors' knowledge, no state-of-the-art work in this field has discussed the non-Normal distribution of noise in triaxial sensors. This is mostly due to the burden of investigating the continuous probability distribution (CPD) that sensor noise follows best, and the simplicity of the likelihood function when assuming sensor noise to follow Gaussian distribution.

In this work, the best CPD that readings of each axis of the magnetometer follow is examined. The challenges in using statistical tests to choose the best distribution are discussed. Furthermore, this paper proposes an algorithm that finds the suitable number of bins for the histogram and the χ^2 -test and only requires knowledge of resolution of the analyzed data.

This paper is organized as follows. Section II introduces properties of the Earth's magnetic field, the characterization of errors and the complete error model. The examination of sensor noise and the best CPDs that readings of each axis follow are shown in III. Section IV explains the calibration procedure and presents results from simulations as well as experiments. Finally, section V summarizes the paper and comments on future work.

Notation: In this paper a denotes a scalar, \mathbf{b} denotes a

vector, and \mathbf{C} denotes a matrix.

II. BACKGROUND

A. Geomagnetism

The geomagnetic field is the magnetic field of the Earth that exists from inside the Earth's core to the outer space. The direction of magnetic field \mathbf{B} at a certain location corresponds to the direction to which the north-pole of a compass needle points. In environments without any magnetic source nearby, the observed magnetic field is the geomagnetic field. Thus, it can support finding the magnetic North at the current location. The geomagnetic field preserves the following useful characteristics

- Intensity: The field ranges from approximately 25 microtesla (μT) in the vicinity of the equator to around 75 μT near the poles [6].
- Variation: The ionosphere's currents and the Earth's interior disturbances cause daily fluctuations of the magnetic field of around 25 nanotesla (nT) and, rarely, superimposed oscillations of about 1 nT in a period of few seconds [6].

Magnetometers in modern smartphones are able to measure the geomagnetic fields, i.e fields with an intensity of 25 to 75 μT . The small variation of the geomagnetic field simplifies the calibration as the change in amplitude of the geomagnetic field in the calibration phase, which is shorter than five minutes is smaller than the resolution of most Microelectromechanical systems based magnetometers. Thus, the Earth's magnetic field in a small region can be considered constant over time.

B. Sources of error

The readings of magnetometers are corrupted by factors from two main categories [3]. The first category represents the instrumentation errors including sensor offsets, scale factor, and non-orthogonality of sensor axes. These errors are due to fabrication limitations. The second category is magnetic deviation. Magnetic deviation is caused by the interference of sensor with ferromagnetic compounds in the vicinity of the host platform. These compounds are divided in to permanent magnetism and induced one or hard iron and soft iron effect respectively. Other types of non-modelled errors, which include generic and more complex effects related to sensor-specific characteristics and magnetic distortions, are out of scope for this paper.

1) Instrumentation errors:

- Sensor offset: the measurement bias $\mathbf{b}_{SO} \in \mathbb{R}^3$ of triaxial sensors in the magnetic-free field.
- Scale factor: the difference in sensitivity of each axis of sensor. This error is formulated as $\mathbf{T}_{SF} \in D^+(3)$, where $D^+(n) = \{\mathbf{A} \in D(n) : \mathbf{A} > 0\}$ and $D(n)$ denotes the set of $n \times n$ diagonal matrices
- Non-orthogonality: the misalignment between axes of sensor and axes of the sensor frame. The effect of non-orthogonality is represented by

$$\mathbf{T}_{NO} = [\epsilon_x, \epsilon_y, \epsilon_z] \in \mathbb{R}^{3 \times 3}$$

2) Magnetic deviation:

- Hard iron: the effect of permanent magnets inherent to the sensor frame, constant bias $\mathbf{b}_{HI} \in \mathbb{R}^3$.
- Soft iron: the effect of soft iron material assumed to attach to the sensor frame of the magnetometer. The induced magnetic field vector \mathbf{h}_{SI} can be presented as a transformation of the Earth's magnetic field, producing

$$\mathbf{h}_{SI} = \mathbf{T}_{SI} \mathbf{h}^S$$

where $\mathbf{T}_{SI} \in \mathbb{R}^{3 \times 3}$ is the soft iron transformation matrix and \mathbf{h}^S is the geomagnetic field in the sensor frame.

C. Complete error model

Instrumentation error and magnetic deviation can be combined into a single model as follows [5]

$$\mathbf{h}_{r,i} = \mathbf{T}_{SF} \mathbf{T}_{NO} (\mathbf{T}_{SI} \mathbf{h}_i^S + \mathbf{b}_{HI}) + \mathbf{b}_{SO} + \epsilon_i, \quad (1)$$

where $\mathbf{h}_{r,i}$ is the magnetometer reading at i^{th} index, r is abbreviation of reading, \mathbf{h}_i^S is the geomagnetic field in the sensor frame, \mathbf{T}_{SF} , \mathbf{T}_{NO} , \mathbf{T}_{SI} , \mathbf{b}_{HI} and \mathbf{b}_{SO} are error sources described in previous sections. $\epsilon_i \in \mathbb{R}^3$ is wideband noise from each axis of sensor. Without loss of generality, the magnetometer reading can be described by

$$\mathbf{h}_{r,i} = \mathbf{T} \mathbf{h}_i^S + \mathbf{b} + \epsilon_i, \quad (2)$$

where $\mathbf{T} = \mathbf{T}_{SF} \mathbf{T}_{NO} \mathbf{T}_{SI}$ and $\mathbf{b} = \mathbf{T}_{SF} \mathbf{T}_{NO} \mathbf{b}_{HI} + \mathbf{b}_{SO}$ denote total transformation and bias effect respectively. Since $\mathbf{T} \in \mathbb{R}^{3 \times 3}$ and $\mathbf{b} \in \mathbb{R}^3$ are unconstrained, unmodelled linear time-invariant magnetic errors and distortions are also taken into account. By finding the Singular Value Decomposition (SVD) of \mathbf{T} , $\mathbf{T} = \mathbf{U} \mathbf{\Sigma} \mathbf{V}^T$, we can define $\mathbf{h}_i^C := \mathbf{V}^T \mathbf{h}_i^S$ as the geomagnetic field in the calibration frame $\{C\}$, which is obtained by the orthogonal transformation \mathbf{V}^T from the sensor frame $\{S\}$. Thus, (2) can be rewritten as

$$\mathbf{h}_{r,i} = \mathbf{U} \mathbf{\Sigma} \mathbf{h}_i^C + \mathbf{b} + \epsilon_i, \quad (3)$$

where \mathbf{U} , $\mathbf{\Sigma}$ and \mathbf{b} are estimated in the calibration process. However, the rotation matrix \mathbf{V} will not be observed in this process if \mathbf{h}_i^S and \mathbf{h}_i^C are not measured. The next section describes how to find the probability distribution functions that noise on each axis of the sensor follows.

III. NOISE EXAMINATION

In this section, all continuous probability distributions available in Matlab R2019a [7] are examined, whether they describe the noise distribution on the three axes of triaxial sensors sufficiently well. In order to be tested with actual sensor data, a chosen distribution had to fulfill two criteria.

- It was not proposed for a specific problem. If the distribution was developed to model a specific phenomena, this should have a relation to intrinsic noise of sensors. For example, Birnbaum-Saunders Distribution is rejected since it was used to model fatigue life of a metal subject to cyclic stress, which is not related to noise in magnetometer measurements.

- The CPD has zero mean or median since there is no reason that noise is more probable to yield positive or negative values. The offset term in (2) already compensates for the non-zero mean/median.

The first criterion reduces the number of suitable CPDs to ten. After the second criterion, the five candidates left to model noise are: Extreme Value, Generalized Extreme Value (GEV), Logistic, Normal and t Location-Scale (tLS) distributions. The measurement plan is introduced in order to check which aforementioned distributions the noises in each axis of the sensor follow.

A. Noise examination setup

1) *Device info:* The sensor used for noise examination was an AK09918 3-Axis Electronic Compass from Asahi Kasei Microdevices Corporation [8]. The sensor is embedded in a HUAWEI P Smart phone with Android operating system. Unlike studies that consider standalone sensor, this setup ensures that signals are affected by similar disturbances as smartphones used in every-day life.

2) *Acquisition Unit:* The AndroSensor application [9] was used to log raw sensor data with a sampling period of 15 ms. Data was stored on the phone and analyzed later on a computer.

3) *Setup:* Data was collected in an open area ($61^{\circ}27'03''N, 23^{\circ}49'01''E$) on the bank of Särkijärvi lake in Tampere, Finland. The site's location was chosen to ensure that no other magnetic fields than the geomagnetic field was measured. Vibration of the Earth at the location was assumed to have negligible effects, which did not distort measurements.

The Android device stayed stationary for 5 minutes. The tests were conducted in 6 different orientations of the sensor frame as shown in Fig. 1 to examine patterns of noise on each axis in 3 Degree of Freedoms (DOFs). Each DOF contains measurements on both positive and negative axes. This measurement setup offers two studies:

- Similarity in true geomagnetic field and noise. For example, without noise the magnetic field readings in the sensor frame on x-axis of orientation 1 should equal readings on y-axis of orientation 2, z-axis of orientation 3 or negative values on y-axis of orientation 4, etc. Secondly, it is possible to study the pattern in noise of different axes measuring the same value such as x-axis of orientation 1 and y-axis of orientation 2.
- Diversity: One axis is used to measure the geomagnetic field in different orientations, e.g. x-axis of the sensor frame is used to measure the magnetic field in 3 DOFs as in orientations 1, 2 and 3.

B. Data anomaly and solution

Measurement readings of one axis in each orientation are the summation of a constant magnetic field value and noise since the sensor was static and the magnetic field was constant (Section II). Histograms are used to represent the shape of the noise distribution on each axis. The documentation of the

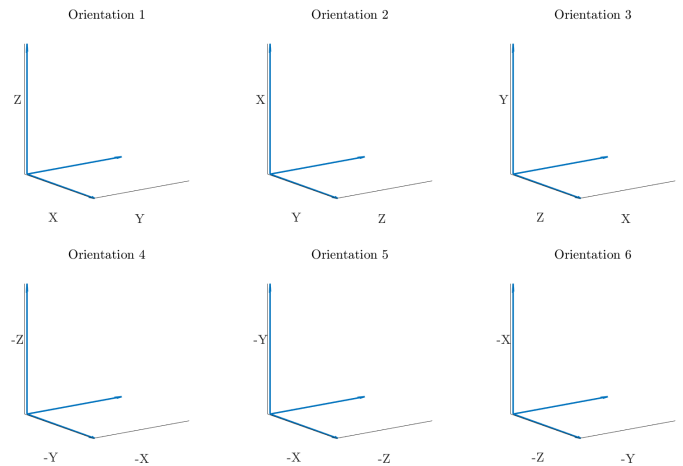


Fig. 1: Noise examination setup

AndroSensor application states that the resolution of raw data from the magnetometer is $0.0625 \mu T$, which is the smallest deviation of measurements. Therefore, readings are grouped to values with $0.0625 \mu T$ discrepancy, i.e. there should be observations every $0.0625 \mu T$ step. For example, the readings of y-axis of orientation 2 contain 1576 observations with value of $13.4375 \mu T$ ($+0$), 1771 of $13.5000 \mu T$ ($+0.0625$), 2080 of $13.5625 \mu T$ ($+2 \cdot 0.0625$), 2170 of $13.6250 \mu T$ ($+3 \cdot 0.0625$) and so on. Although this repetition should remain, there are no observations for $13.6875 \mu T$ ($+4 \cdot 0.0625$). This leave-one-out every 5-bin pattern is observed again in the next 5 bins and also in the whole dataset. Choosing the appropriate bin widths (or number of bins) for the histogram can fill this gap with observations without assuming the original of problems nor distorting the readings by interpolation. To determine the greatest number of bins such that the histogram contains no empty bins, Algorithm 1 is proposed.

Algorithm 1 Maximal approved number of bins

Input: Magnetometer measurements of t-axis h_r^t

Resolution of AndroSensor: $r = 0.0625 \mu T$

Output: The suitable number of bins n_{suit}

1. $M = \max(h_r^t); m = \min(h_r^t)$

2. $n_M = \lceil \frac{M-m}{r} \rceil; n_m = \lfloor \frac{M-m}{2r} \rfloor$

3.

For $n = n_M : -1 : n_m$

If histogram of h_r^t with n bins contains no empty bins:

$n_{suit} = n;$

break;

end

The histogram may also have no empty bins by choosing smaller number of bins, however, at least some bins will have more measurements. Thus, this algorithm also guarantees that the histogram does not aggregate data unnecessarily, which might hide the pattern describing the distribution.

C. Fitting probability distributions

The probability density functions (PDFs) of the five chosen CPDs are functions of two or three parameters. For instance, the Normal distribution is described by mean and standard

TABLE I: Results of fitting probability distributions to noise on all three axes, measured in six different orientations. Two statistical tests were used. For each pair of axis and orientation, D_1/D_2 are the best and second best distributions for describing the observed noise.

Axis Orientation	χ^2			Kolmogorov-Smirnov		
	X	Y	Z	X	Y	Z
1	L/T	T/N	T/N	T/N	N/G	N/T
2	T/L	N/T	G/T	N/T	N/T	G/L
3	T/N	N/T	N/T	N/T	N/T	L/T
4	T/N	G/N	G/I	N/T	G/L	G/L
5	T/N	T/N	N/T	N/T	T/N	N/T
6	T/N	I/I	G/I	N/T	G/L	G/T

G: Generalized Extreme Value, L: Logistic, N: Normal, T: t Location-Scale, I: Inconclusive.

deviation while the t Location-Scale distribution is described by three parameters: location, scale and shape. The built-in Matlab function "fitdist" based on the MLE framework is used to estimate those parameters. The five CPDs are created and compared visually with readings of each axis by "probplot" and "qqplot" functions [7]. In those plots, most measurement readings fall on one side of Extreme Value distribution reference line, indicating that the Extreme Value distribution is not a suitable distribution [13].

Algorithm 1 is applied to data of each axis, for all six orientations. The data is then grouped to bins and evaluated by the χ^2 and the Kolmogorov-Smirnov tests [7]. In the χ^2 test, a greater significance level α means that the CPD fits the noise better. Similarly, the larger the p-value, the better a CPD fits the noise in the other test. The best and second best probability distributions according to α or p-value that noise on the three axes follows is shown in TABLE I. When values of α of two distributions are underflow and using the criteria of g value cannot choose which distribution is better, the result is inconclusive [13].

The distribution that is the best fit over all six orientations most often is chosen for each axis. If two distributions have the same number of times being the best, the one with more times being second best is chosen. Without the latter, it is not possible to choose the best distribution, e.g. in the χ^2 -test on Y axis, both the Normal and t Location-Scale are two times being the best fit. According to the χ^2 -test, t Location-Scale is the best distribution that models noise on x-axis (5 times best, 1 time second), Normal is the best distribution that noise on y-axis (2 times best, 3 times second) follows while Generalized Extreme Value is most suitable for z-axis (3 times best). Kolmogorov-Smirnov test yields a different conclusion, Normal is the best for both x (5 times best, 1 time second) and y (3 times best, 1 time second) axes while best distribution for z-axis is the same as χ^2 -test result. A table containing the α or p-value (including the g values) of all tested four distributions for all six observations and both tests can be found from [13].

IV. MAGNETOMETER CALIBRATION ALGORITHM

The results of the previous section allow us to model noise of each axis $[\epsilon_{x,i} \ \epsilon_{y,i} \ \epsilon_{z,i}]^T$ by the corresponding distribution. It is known that the correlation in noise between two axes requires further study and there exist a disagreement between the

two statistical tests. Thus, to simplify the derived mathematical steps and just to show how the calibration works, we assume that noise on each axis is Gaussian with zero mean, identical standard deviation and independent to each other. The noise terms are now

$$\epsilon_i \sim \mathcal{N}(\mathbf{0}, \sigma^2 \mathbf{I}_{3 \times 3}) \stackrel{(3)}{\implies} \mathbf{h}_{r,i} \sim \mathcal{N}(\mathbf{U}\Sigma\mathbf{h}_i^C + \mathbf{b}, \sigma^2 \mathbf{I}_{3 \times 3}). \quad (4)$$

The MLE is used to maximize the conditional probability of observed values given parameters $(\mathbf{U}, \Sigma, \mathbf{b}) \in O(3) \times D^+(3) \times \mathbb{R}^3 := \Theta$ and $\mathbf{h}_i^C \in S(3), i = 1, \dots, n$ where $S(3)$ is the set of 3D vectors whose length is 1 and $O(n)$ is the set of $n \times n$ orthogonal matrices.

$$\begin{aligned} & \max_{(\mathbf{U}, \Sigma, \mathbf{b}) \in \Theta} p\{\mathbf{h}_{r,i} | \mathbf{U}, \Sigma, \mathbf{h}_i^C, \mathbf{b}\} \\ & \mathbf{h}_i^C \in S(3), i=1, \dots, n \\ & \epsilon_i = \mathbf{h}_{r,i} - \mathbf{U}\Sigma\mathbf{h}_i^C - \mathbf{b} \\ & \text{i.i.d. (4)} \quad \max_{(\mathbf{U}, \Sigma, \mathbf{b}) \in \Theta} \prod_{\mathbf{h}_i^C \in S(3)} \prod_{i=1}^n \frac{e^{-\frac{1}{2}\epsilon_i^T (\sigma^2 \mathbf{I})^{-1} \epsilon_i}}{(2\pi|\sigma^2 \mathbf{I}|)^{1/2}} \\ & = \min_{(\mathbf{U}, \Sigma, \mathbf{b}) \in \Theta} \sum_{\mathbf{h}_i^C \in S(3)} \prod_{i=1}^n \left\| \Sigma^{-1} \mathbf{U}^T (\mathbf{h}_{r,i} - \mathbf{b}) - \mathbf{h}_i^C \right\|^2. \quad (5) \end{aligned}$$

The minimum of (5) is computed iteratively using Newton-like or gradient methods. However, the search space is large since we need to estimate n magnetic field vectors \mathbf{h}_i^C . The search space is then $2n + \dim(\Theta) = 2n + \dim(O(3)) + \dim(D^+(3)) + \dim(\mathbb{R}^3) = 2n + 9$. The minimization problem (5) can be rewritten to search only in the parameter space Θ since the solution $(\mathbf{U}^*, \Sigma^*, \mathbf{b}^*)$ also minimizes

$$\min_{(\mathbf{U}, \Sigma, \mathbf{b}) \in \Theta} \sum_{i=1}^n \left(\left\| \Sigma^{-1} \mathbf{U}^T (\mathbf{h}_{r,i} - \mathbf{b}) \right\| - 1 \right)^2. \quad (6)$$

Finally, minimization problem (6) can be formulated on the Euclidean space, which allows for the use of optimization tools for unconstrained problems [10]

$$\min_{\mathbf{A} \in \mathbb{R}^{3 \times 3}, \mathbf{b} \in \mathbb{R}^3} \sum_{i=1}^n \left(\left\| \mathbf{A} (\mathbf{h}_{r,i} - \mathbf{b}) \right\| - 1 \right)^2, \quad (7)$$

with the solution as $\mathbf{A}^*, \mathbf{b}_A^*$, where \mathbf{A}^* is the SVD decomposition $\mathbf{A}^* = \mathbf{U}_A^* \Sigma_A^* \mathbf{V}_A^{*T}$. The solution of (6) is given by $\mathbf{U}^* = \mathbf{V}_A^*, \Sigma^* = \Sigma_A^{*-1}, \mathbf{b}^* = \mathbf{b}_A^*$. A good initial guess can reduce the number of iterations and time for finding the optimal solution. In Matlab, an algorithm is implemented by Barraud and Lesecq [11], which yields two coefficients \mathbf{X}, \mathbf{y} that can be used directly as initial guess $\mathbf{A}_0 = \mathbf{X}, \mathbf{b}_0 = \mathbf{y}$ in optimization problem (7).

A detailed derivation for getting from (4) to (7) can be found from [5]. This derivation shows that with the Gaussian distribution assumption for noise, the computational complexity of the algorithm can be reduced tremendously. Without this assumption, the search space is $(2n + \text{number of parameters of chosen distributions})$ and the reduction of mathematical complexity requires further study.

Given the optimal solution of (7) as $\mathbf{U}^*, \Sigma^*, \mathbf{b}^*$, the unbiased unit norm vector representing the Earth magnetic field in the calibration frame $\{C\}$ is obtained by manipulating (3)

$$\mathbf{h}_i^C = \Sigma^{-1} \mathbf{U}^T (\mathbf{h}_{r,i} - \mathbf{b}). \quad (8)$$

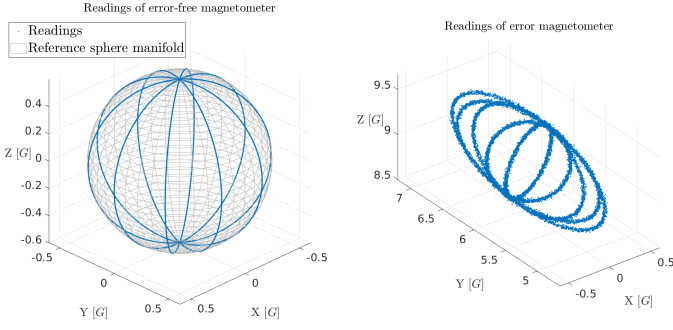


Fig. 2: Simulated data of true(left) and distorted magnetic field

In order to find the geomagnetic field in the sensor frame $\{S\}$, one needs the alignment procedure represented by rotation matrix \mathbf{V} mentioned in Section II. This alignment is independent from the calibration procedure. It requires external heading sources or localization systems. In [5], the step by step procedure to obtain \mathbf{V} in the Least Square framework is discussed. The estimated $\hat{\mathbf{V}}$ helps transforming measurements from the calibration frame $\{C\}$ to an Optimized-Sensor $\{OS\}$ frame. Next, simulation and experimental results are shown to demonstrate the effect of the calibration procedure.

A. Simulation result

Simulated data is used to analyze the efficiency of the calibration algorithm. The randomly picked values of parameters of error sources described in Section II are

$$\mathbf{T}_{SF} = \text{diag} \left(\begin{bmatrix} 1.0 \\ 1.5 \\ 1.2 \end{bmatrix} \right), \mathbf{T}_{NO} = \begin{bmatrix} 1.000 & 0.000 & 0.000 \\ 0.174 & 0.985 & 0.000 \\ -0.174 & 0.086 & 0.981 \end{bmatrix},$$

$$\mathbf{T}_{SI} = \begin{bmatrix} 0.58 & -0.73 & 0.36 \\ 1.32 & 0.46 & -0.12 \\ -0.26 & 0.44 & 0.53 \end{bmatrix}, \mathbf{b}_{HI} = \begin{bmatrix} -1.5 \\ 4.0 \\ 2.0 \end{bmatrix} G,$$

$$\mathbf{b}_{SO} = [1.5 \ 0.4 \ 6.0]^T G, \mathbf{h}^{LLF} = [0.0 \ 0.0 \ 0.6]^T G$$

The artificial magnetometers are supposed to rotate 360° around the z-axis in Local Level Frame (LLF), i.e. sweep yaw angle $\in [0, 360]^\circ$, and 180° around the x-axis (sweep pitch angle). In total, 10^4 measurements are produced with additive zero-mean, 10 mG standard deviation Gaussian noise. Fig. 2 shows the simulated data for an error-free magnetometer with norm of 0.6 G on the left and for an erroneous magnetometer (using the error parameters from above) on the right.

The likelihood function f is normalized by the number of samples n . Function "fminunc" in Matlab is used for this unconstrained optimization problem. Default values are used for the step size and the terminal condition. Quasi-Newton iterative algorithm is used. As mentioned earlier, the calibrated magnetic measurement is in the calibration frame, it is not aligned with true magnetic field in the sensor frame (left panel of Fig. 3). In real-world situations, the sole calibration algorithm should help determining the heading angle of the magnetometer without being aligned constantly by using an external source. Given the first 2000 noiseless magnetic measurements in the sensor frame, one can

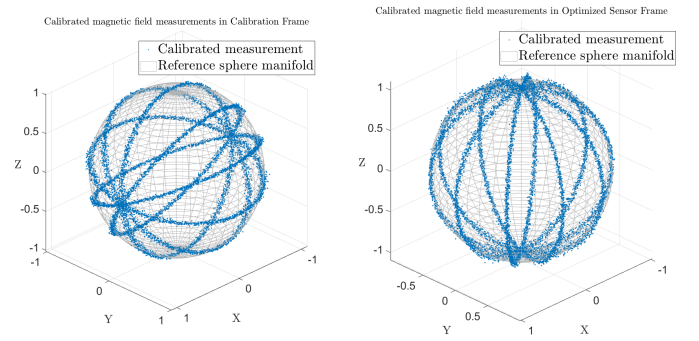


Fig. 3: Simulation data of Calibrated magnetic field in Calibration and Optimized Sensor Frame

TABLE II: Calibration results

$f(x_e)$	$f(x_0)$	$f(x^*)$	b_{LS}	b_{MLE}
97.3626	4.03×10^{-4}	4.01×10^{-4}	4.79×10^{-4}	4.13×10^{-4}

already estimate the orthogonal matrix \mathbf{V} from the alignment procedure to transform the remaining 8000 noisy calibrated measurements from $\{C\}$ frame to $\{OS\}$ frame. As shown in Fig. 3, the calibrated measurements in the $\{OS\}$ frame is in the similar orientation as the ones on the left of Fig. 2. Note that axes of Fig. 3 contain no units since calibrated measurements \mathbf{h}_i^C and \mathbf{h}_i^{OC} are in the unit sphere. Provided the norm of the geomagnetic field (0.6 G), the aligned-calibrated measurements are then multiplied by that norm. The mean value of Euclidean distance of 8000 noiseless geomagnetic field in the sensor frame and the calibrated measurements in the $\{OS\}$ frame after multiplied is

$$\frac{1}{8000} \sum_{i=2001}^{10000} \|\mathbf{h}_i^S - 0.6\mathbf{h}_i^{OS}\|_2 \approx 16 \text{ mG},$$

which is comparable to the standard deviation of added noise. Let us define the Euclidean distance between the estimated and true parameters, $b_{LS} = \|\mathbf{b}_0 - \mathbf{b}\|_2$ and $b_{MLE} = \|\mathbf{b}^* - \mathbf{b}\|_2$. TABLE II shows that the likelihood function $f(x_e)$ is very large for non-calibrated data. Initial guess improves likelihood function $f(x_0)$ more than 10^5 times while the calibration procedure further reduces likelihood function ($f(x^*)$). With only 29 iterations, the accuracy of estimated parameter \mathbf{b}^* is improved by 14% compared to \mathbf{b}_0 .

B. Experimental result

The experimental device was the same as the one used in Section III. The acquisition unit and its properties remained.

At the same location as in Section III, the device was rotated in a random manner to cover the full ellipsoidal manifold when it was recording. The norm of the reference geomagnetic spherical manifold on measurement day was extracted from the WMM geomagnetic model [12] with the given coordinates. Fig. 4 shows the magnetic field measurements and the reference geomagnetic-norm sphere.

In Fig. 4, the most trivial error effect is the combination of sensor sensitivity and soft iron since the raw measurements fall out of the reference sphere. Only four iterations are needed to find the calibration parameters, the found bias term is

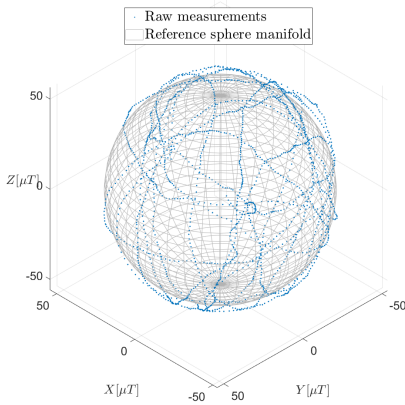


Fig. 4: Measurements of the magnetic field when rotating the device arbitrarily and the geomagnetic-norm sphere reference

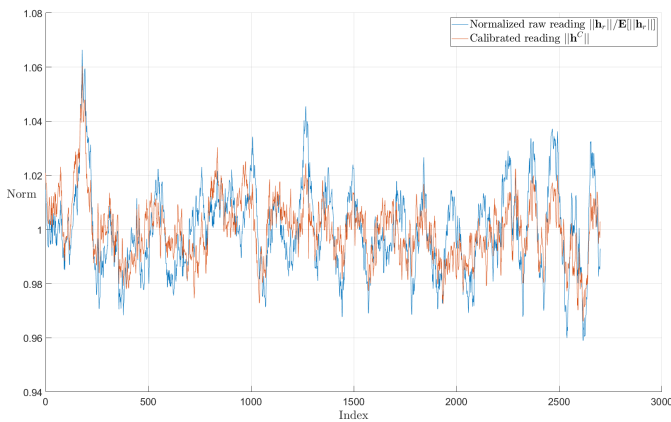


Fig. 5: Norm of calibrated data compared to raw data

$\mathbf{b}^* = [-0.06, -0.17, 0.06]^T \mu T$. The bias term is small since there are no external magnetic sources nearby. The error matrices such as Non-orthogonal, Scale factor cannot be separated from the estimated matrices. Hence, it is not worth showing values of Σ and \mathbf{U} since they provide no information for the error sources. The norm of the calibrated magnetometer data is compared with the norm of normalized raw data as shown in Fig. 5. With a standard deviation of 0.011 for calibrated norm and 0.016 for normalized raw data, the calibration algorithm reduce the variation by more than 30%. It thus enables denoising and partially compensates errors.

V. DISCUSSION AND OUTLOOK

The proposed algorithm for finding optimal bin width requires only knowledge of the resolution of the data but not the distribution of the data itself. It ensures that there are no empty bins, which is necessary for finding the level of significance in the χ^2 -test. Although state-of-the-art research assumes measurement noise for triaxial sensors to follow the same Normal distribution on all three axes, statistical tests in this paper disprove this assumption. Further developments of the likelihood function are needed. At least, Normal distributions with different standard deviations for each axis should be studied. Due to the abnormality in sensor reading being application-dependent, further research analyzing this irregularity is required.

Without a good initial guess, solving the unconstrained optimization problem by "fminunc" function in simulation data also showed that the estimated result can be far from the true result. The reason for this poor performance is that the likelihood function is non-convex and therefore might get stuck at a local minimum.

The calibration algorithm reduced the uncertainty in magnetic measurements in the experiment. In order to obtain lower standard deviation, better probability distributions should be chosen for noise on each axis. However, because the best CPDs founded by the χ^2 -test are different from those found by the Kolmogorov-Smirnov test, no final decision on which distributions to use was made. The Akaike information criterion that was founded on information theory will be, in that case, a better standard to evaluate the best fitted distributions. After choosing the best fitted distribution for each axis, the new likelihood function could be derived. Then, further mathematical manipulations could be developed for this specific case to simplify the optimization function.

Simulation data demonstrated the effects of each error type by matrices and the calibration algorithm compensated the influence of those effects. Using a part of true readings as reference heading sources shows the applicable scenario: The magnetometer only needs heading information for a short time, then it can self calibrate and align. The experimental data, likewise, shows the effect of calibration method. The interference of error sources are not trivial since the readings almost fall on the sphere. This means, that the errors of the used magnetometer, which was launched in 2017, are less significant than those experienced by older magnetometers.

REFERENCES

- [1] National Geospatial-Intelligence Agency, "The American Practical Navigator: Bowditch". Skyhorse Publishing Company, Incorporated, 2013. ISBN: 9781620877968
- [2] Foster, Christopher C and Elkaim, Gabriel Hugh, "Extension of a two-step calibration methodology to include nonorthogonal sensor axes," *IEEE Transactions on Aerospace and Electronic Systems*, vol. 44, no. 3, pp. 1070–1078, 2008
- [3] Renaudin, Valérie and Afzal, Muhammad Haris and Lachapelle, Gérard, "Complete triaxis magnetometer calibration in the magnetic domain," *Journal of sensors*, vol. 2010, 2010.
- [4] P. Guo, H. Qiu, and Y. Yang, "The soft iron and hard iron calibration method using extended Kalman filter for attitude and heading reference system," *IEEE Position Location Navig. Symp.*, pp. 1167–1174, 2008
- [5] Vasconcelos, JF and Elkaim, G and Silvestre, C and Oliveira, P and Cardeira, B, "A geometric approach to strapdown magnetometer calibration in sensor frame," *IFAC Proceedings Volumes*, vol. 41, no. 1, pp. 172–177, 2008
- [6] Janez Stepisnik, "NMR down to Earth," *Nature, International journal of science*, vol. 800, no. 439, pp. 799, 2006
- [7] MATLAB, ver. 9.6.0.1072779 (R2019a), pub. The MathWorks Inc.
- [8] Magnetometer Sensor. Available: <https://www.digikey.com/catalog/en/partgroup/ak09918/70323>, access date 2019-05-20
- [9] AndroSensor application. Available: <https://play.google.com/store/apps/details?id=com.fivasim.androsensor&hl=en>, access date 2019-05-01
- [10] Fletcher, Roger, "Practical methods of optimization," *John Wiley & Sons*, 2013
- [11] Least Square magnetic calibration toolbox. Available: https://se.mathworks.com/matlabcentral/fileexchange/23398-magnetometers-calibration?s_tid=prof_contriblnk
- [12] NCEI Geomagnetic Calculators. Available: <https://www.ngdc.noaa.gov/geomag/calculators/magcalc.shtml#igrfwmm>, access date 2019-05-20
- [13] Nhan Nguyen, "The Statistical Analysis of Noise in Triaxial Sensor", Bachelor's Thesis, *Tampere University*, 2019. Available: <http://urn.fi/URN:NBN:fi:tuni-201909053161>